CONF-950682--5

Modeling of Thermomechanical Conditions in Sigmajig Weldability Test

Z. Feng, T. Zacharia and S. A. David
Metals and Ceramics Division, Oak Ridge National Laboratory
P. O. Box 2008, Oak Ridge, TN 37831-6140

DISCLAIMER

DISCLAIMER

Portions of this document may be illegible in electronic image products. Images are produced from the best available original document.

Abstract

A finite element model has been developed to evaluate quantitatively the thermomechanical conditions for weld metal solidification cracking of a nickel based superalloy single-crystal in a laboratory weldability test, namely, the Sigmajig test. The effects of weld pool solidification on the thermal and mechanical behaviors of the specimen were considered. Stress-temperature-location diagrams were constructed to reveal the complex local stress development at the trailing edge of the weld pool. The calculated local stress in the solidification temperature range is used to explain the experimentally observed initiation of solidification cracking of the single-crystal under different welding and loading conditions, based on the material resistance versus the mechanical driving force.

The Sigmajig test (1) is a hot cracking test commonly used for sheet metal. The test uses a pre-applied load during welding and determines a threshold stress above which a centerline crack initiates. The consensus is that (i) the higher the threshold stress, the more resistant to cracking the alloy will be; (ii) a crack is not expected in the Sigmajig test when the pre-applied stress level is below the alloy's cracking threshold stress. The threshold stress has been shown to be sensitive to the variations in alloy composition, welding process and parameters, and is used as a quantitative index for an alloy's susceptibility to cracking. In the past, few attempts have been made to correlate the external pre-applied stress to the local stress/strain field at the crack initiation site.

In the development of a nickel-based superalloy, the weldability of the alloys was characterized using the Sigmajig test. When the test was conducted without applying a load, some alloy compositions exhibited severe tendency for weld centerline solidification cracking. However, with pre-applied load, the threshold stress values could be measured as high as 200 MPa. Similar results were also reported for FeAl alloys (2). These experimentally observed phenomena are difficult to interpret without considering the local stress/strain conditions at the trailing edge of the moving weld pool.

As a continuing effort to quantify the thermomechanical contribution to solidification cracking, this study provides a detailed finite element analysis of the dynamic development of the local thermal stresses at the trailing edge of the moving weld pool that influence the formation of solidification cracking in the Sigmajig test. The aim of the study is to relate the experimentally observed crack initiation behavior under various welding and loading conditions to the local stress evolutions calculated from the thermomechanical models.

Experimental

Material. The material used in this study was an experimental nickel-based superalloy single-crystal with composition similar to that of IN-738. The 0.787 mm (0.031 in) thick, 50x50-mm (2x2-in) square Sigmajig test specimens were cut from a single-crystal casting in the plane normal to the [001] crystal growth direction. The edges of the specimen were along [100] and [010] directions. The dendritic microstructure of the casting was preserved in the specimen prior to welding. The bulk liquidus and solidus temperatures of the alloy were determined to be 1601 and 1404 K respectively, using differential thermal analysis (DTA).

Welding and Sigmajig Testing. An autogenous gas tungsten arc (GTA) weld was made along the centerline of a specimen, i.e., along the [100] crystallographic direction of the single-crystal. The welding was performed using a Hobart Cyber-Tig II welding power source and an 1.6 mm (1/16 in), 2% thoriated tungsten electrode. Two welding speeds, 4.23 mm/s (10 in/min) and 14.8 mm/s (35 in/min), were selected to study the effect of welding speed on the occurrence of cracking. The welding current was set at 32 A for the low welding speed (4.23 mm/s), and 75 A for the high welding speed (14.8 mm/s). The arc length was set at 0.787 mm (0.031 in). Dependent upon the welding speed, the arc voltage varied from

10 to 10.5 V in the high speed tests and 8.5 to 9.5 V in the low speed tests. Argon shielding gas with a flow rate of 1.42 cm^3/s was applied to the top surface of the specimen. The copper chill block usually placed beneath the specimen to control the weld width was removed during the test in order to avoid analyzing the complex contact heat loss from the block. With the above welding parameters, full penetration welds were obtained in all tests.

Two pre-stress levels were selected: 68.9 MPa (10ksi) and 172 MPa (25ksi). In addition, some specimens were welded without the fixture by laying the specimen down on the steel grips, eliminating the constraining effect from the loading fixture. A total of six combinations of loading (constraint) and welding conditions were investigated.

Computational Model

The thermomechanical behavior of the specimen during welding was modeled using the uncoupled approach, because the dimensional changes are negligible and the mechanical work done is insignificant compared to the thermal energy from the welding arc (3,4). It was further assumed that the specimen does not crack in the mechanical model. Finite element formulation formed the basis for this analysis.

Heat Transfer Model. In light of the thickness of the specimen, the heat transfer in the specimen was modeled as a two-dimensional heat conduction problem. A symmetric half of the single-crystal sheet was discretized with 4-node linear isoparametric quadrilateral elements which are more suitable for problems involving the latent heat effect. Smaller elements were used near the fusion zone. In addition, it was assumed that the steel grips had negligible effect on the temperature distribution of the specimen and thus were not included in the heat transfer analysis.

Following the approach in (5), all of the boundary conditions, i.e., the heat loss from the specimen surfaces and the heat flux from the arc, were incorporated into the heat diffusion equation in terms of internal heat generation or loss (body heat flux). The heat flux from the moving welding arc was assumed to have a spatial distribution of radial symmetric Gaussian profile in the plane of the plate, but uniformly distributed over the entire thickness of the plate. A constant arc efficiency of 70% was used for GTAW. The arc beam radius was taken to be the same as the electrode diameter (1.6 mm).

The convective and radiative heat losses from the surfaces of the plate were considered, whereas the heat loss from the edges of the plate was ignored. The convective heat transfer coefficient and the radiative emissivity was assumed to be 84 W/m^2K, and 0.2, respectively.

Due to the experimental nature of the single-crystal used in the study, the thermophysical properties were not readily available. The values adopted in the computational analyses were the average values based on the data for several superalloys with similar compositions (6-8). Temperature dependent thermal conductivity and specific heat were used. In order to account for the increased convective heat transfer by the molten metal flow in the weld pool, the thermal conductivity was enhanced linearly from the solidus to the liquidus and remained constant above the liquidus. The conductivity value for the liquid was five times that at the solidus temperature. A constant density of 8.11 g/cm^3 was taken for the entire temperature range. The latent heat of fusion was assumed to be 297.6 J/g.

Generally speaking, the latent heat release rate during weld solidification is not a constant and can be related to the compositions and cooling rate by consideration of the solidification kinetics during welding (5). However, for the experimental alloy used in this study, necessary thermophysical data were not available for such a treatment. The following simplified approach was used instead in the heat transfer analysis.

The solidification temperature range (1601-1404 K) of the alloy was evenly divided into three intervals. The latent heat was assumed to be released in these three intervals by a ratio of 7:2:1, with a major portion of the latent heat being released in the first interval:

$$q_i = \begin{cases} 0.7\dfrac{3L}{T_l - T_s}\dfrac{dT}{dt} & for \quad T \in (1535,1601K) \\ 0.2\dfrac{3L}{T_l - T_s}\dfrac{dT}{dt} & for \quad T \in (1470,1535K) \\ 0.1\dfrac{3L}{T_l - T_s}\dfrac{dT}{dt} & for \quad T \in (1404,1470K) \end{cases} \qquad (1)$$

where L is the volumetric latent heat, and T_l and T_s the liquidus and solidus of the alloy, respectively. This treatment was consistent with many experimental observations (9) and analyses (10) in which the solidification rate is highest at the early stage of solidification.

Mechanical Model. The mechanical responses of the superalloy specimen during the Sigmajig test were considered as a geometrically nonlinear plane stress problem. Non-zero stress components only exist in the plane of the specimen. In those cases where pre-stress was applied, the steel grips of the Sigmajig fixture were also included in the model, with the same plane stress assumption but a different thickness (38 mm). It was assumed that there was no relative displacement between the steel grips and the testing plate.

Similar to the heat transfer analysis, only half of the specimen needed to be modeled due to the symmetry with respect to the weld centerline (Figure 1). The specimen and the steel grips were discretized with eight-node second order isoparametric quadrilateral elements with a reduced integration scheme.

In the Sigmajig test, a specimen is pre-stressed by a pair of steel bolts before welding. The pre-stress is maintained by two stacks of Bellville washers in the load train, which had a displacement/load curve with a slope of 6.167×10^{-4} mm/N (0.108 mils/lbf) for each stack of washers (1). This loading arrangement was effectively modeled in this study as a pair of "push" springs (Figure 1). After some simple manipulation, the following equation was derived to describe the load and displacement relation of a push spring during welding:

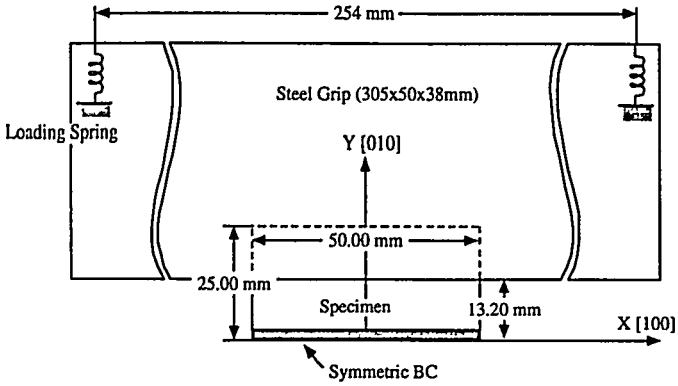

Figure 1 - Geometric representation of the Sigmajig test and boundary conditions in computational models

$$F = 1621.4u - 135.73\sigma_o \quad (2)$$

where F (N) is the force in the spring, u (mm) the displacement of the spring, relative to its position after preloading. σ_o (ksi) is the prescribed stress level for a given test. It was assumed that the springs could only move along the y-direction, i.e., normal to the weld centerline. Because of the thermal expansion/contraction of the specimen, the actual stress applied to the specimen by the loading train was expected to fluctuate around the pre-stress level during the test.

According to the data for several nickel-based superalloys (8,11,12), the elastic constants are not strong functions of composition. Thus, the single crystal elastic constants used in this study were based on pure Ni (12) and extrapolated for temperatures above 900K.

However, the plastic constitutive relation for the experimental single-crystal alloy was not available. This study used a rather simplified temperature dependent isotropic linear work-hardening constitutive relation with a plastic modulus of $2\sigma_{ys}$. σ_{ys} is the initial yield strength of the alloy similar to those of IN-738.

As discussed in (5), the effects of solidification in the GTA weld pool need special considerations when the mechanical responses of a welded structure are formulated on the basis of the continuum mechanics of solid. In place of the tedious dynamic element rebirth scheme used in (5), two effects - the annihilation of plastic strain upon solidification and the change of initial temperature in thermal strain calculation - were treated by modifying the material constitutive relation in the solidification temperature range in this study. Special attention was paid to avoid the possible numerical convergence difficulties that could rise due to the drastic changes of plastic and thermal strains upon solidification.

Results and Discussions

Sigmajig Test. Both centerline (longitudinal) and transverse cracks were observed in this study. Figure 2 shows the welds with cracks in some selected specimens. Table 1 summaries the occurrence of the centerline cracking under the conditions investigated. The severity of the centerline cracking is represented by the percent cracking, defined as fraction of the specimen length cracked. As indicated in the table, the crack length and initiation site for centerline cracking depends on both the arc welding speed and the pre-stress level. Cracks were observed in three cases: (i) low welding speed and high pre-stress (4.23 mm/s, 172 MPa); (ii) high welding speed and high pre-stress (14.8 mm/s, 172 MPa); and (iii) high welding speed and zero pre-stress (14.8 mm/s, stress-free). Cracks initiated at the start of the weld when the welding speed was high. On the other hand, centerline cracking did not initiate until the solidification front passed the middle point of the plate in the low welding speed tests.

The observation of the transverse cracks was quite unusual, since the Sigmajig test was designed for testing the susceptibility of centerline cracking. The tendency for the transverse cracking seems dependent upon the welding speed only. Severe transverse cracking occurred in the high speed welding (14.8 mm/s) tests with an average of 7 cracks per specimen, whereas only 3 or less cracks were observed in each low welding speed specimen, regardless the loading condition.

Numerical Analysis. As noted earlier, the bulk liquidus and solidus temperatures measured from DTA for the alloy investigated are 1601 and 1404 K respectively. It is expected that the actual solidus during weld metal solidification would be lower than 1404K due to the non-equilibrium solidification process involved. Direct observation of the solidification cracking of Type 316 stainless steel in Sigmajig test (13) has revealed that the weld centerline cracking often initiated at a location some distance behind the apparent trailing edge of the weld pool, i.e., at a temperature below the bulk solidus of 316 steel (1645K, according to (14)). Solidification cracking could also initiate at a higher temperature, even reach the apparent solidus temperature when the external loading rate is high, as noted by Matsuda *et al* (9). This study assumes that, depending upon the testing conditions, cracking would initiate anywhere between 1600 and 1300K as long as the stress/strain condition and the microstructure at that particular temperature favor such an event. Therefore, this study will focus on the local stress evolution over the entire temperature range between 1600 and 1300K.

Weld metal solidification cracking results from the competition between the material resistance to cracking and the mechanical driving force for cracking. When the mechanical driving force exceeds the material resistance, cracking occurs. The parameters representing the mechanical driving force for solidification cracking may be a complex function of the stress and strains in the solidification temperature range. As a first approximation, this study assumed that the stress transverse to weld centerline is responsible for the occurrence of centerline cracking, and the longitudinal stress for the transverse cracking. It is worth noting that other simple parameters have been used also, for example, the mechanical strains accumulated in the solidification temperature range (5,15).

Table 1 Percent of Centerline Solidification Cracks

Pre-stress Level (MPa)	Welding Speed	
	4.23 mm/s	*14.8 mm/s*
Stress-free	0%	15%**
68.9	0%	0%
172	50%*	100%

* Crack initiated approximately at the middle point of the weld
** Crack initiated at the start of the weld

Although the material resistance to cracking (the threshold value of stress or strain to initiate crack) varies with changes in welding speed, heat input, location, composition, etc., it is reasonable to assume that the material resistance is independent of the pre-loading condition in the Sigmajig test. This forms the basis for comparing the mechanical driving forces under different loading conditions used in this study.

Stresses at the Centerline Crack Initiation Sites. For the purpose of determining the mechanical driving force for centerline crack initiation, it is important to examine the stress evolution for all positions along the centerline in the crack initiation temperature range. To this end, transverse stress-location-temperature diagrams were generated from the computational analysis for each of the six testing conditions. Figure 3 shows as an example the diagram for the low welding speed and high pre-load case. The diagram was constructed by tracing the transverse stress evolution of each nodal point on the centerline as the temperature decreases from 1600K to 1300K.

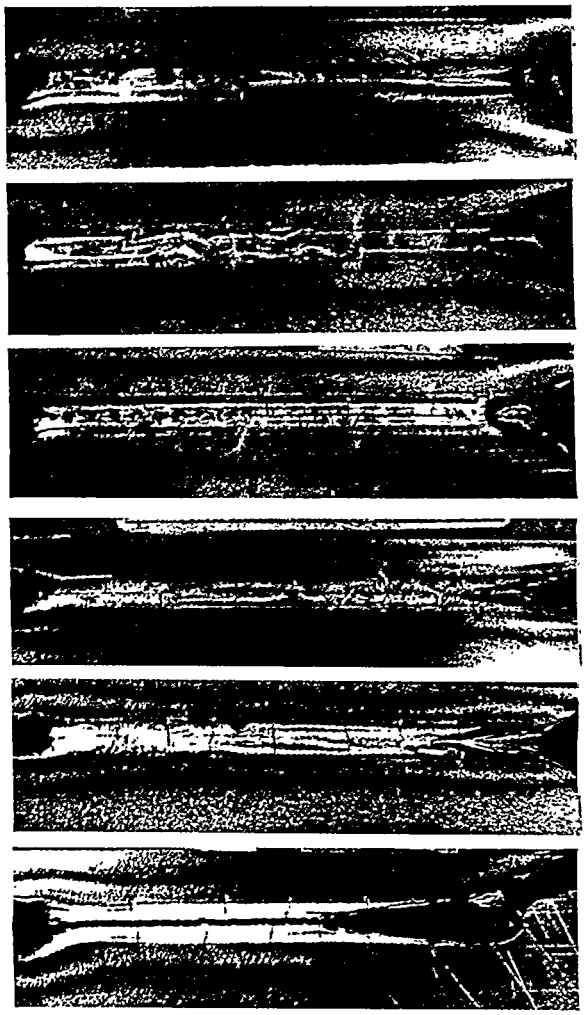

Figure 2 - Appearance of welds and solidification cracks. Welding direction was from left to right. From top to bottom: 4.23mm/s, free; 4.23mm/s, 68.9MPa; 4.23mm/s, 172MPa; 14.8mm/s, free; 14.8mm/s, 68.9MPa; 14.8mm/s, 172MPa

The transverse stress patterns in the specimen are quite complex. Most importantly, the local stress distributions in the vicinity of a weld pool, particularly around the trailing edge of the weld pool, are greatly influenced by the location of the weld pool in the specimen, even for a given testing condition. In general, the evolution of the transverse stress at a point on the weld centerline is such that a compressive stress is first developed upon cooling from the liquidus temperature of the alloy. In the region around the starting edge of the specimen, this compressive stress normally changes to a tensile stress before the completion of solidification. As the weld pool moves inward from the starting edge of the specimen, the transition to the tensile stress gradually shifts down to lower temperatures. In certain loading and welding conditions, the compressive stress dominates the entire crack initiation temperature range (1600 to 1300K). This general trend is consistent with other recent computational studies on the local stress distributions around a traveling weld pool (5,10,13). However, the development of a second tensile stress hump after the solidification front passes the middle point of the specimen as shown in Figure 3 has not been reported in the past. The location of this second tensile stress hump depends upon welding speed and loading conditions. For the case shown in Figure 3, the site where the hump first breaks into tension is located at about 30 mm from the starting edge of the specimen (x=5mm). The transition to tensile stress shifted further away from the weld starting edge in the low welding speed cases. As the pre-stress further increases, this tensile stress hump shifts toward the middle point of the specimen.

A fundamental characteristic of centerline solidification cracking in the Sigmajig test is that it is very rare to have a crack length between 60% to 100% (1). This means that the

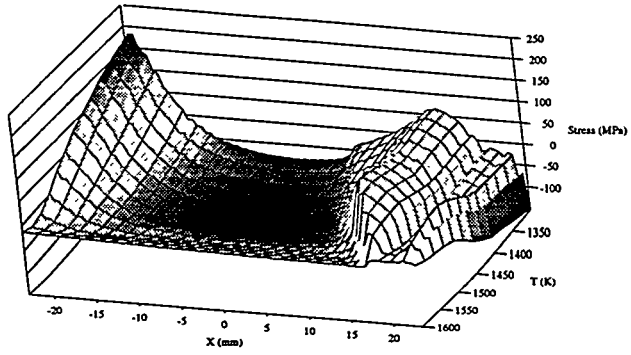

Figure 3 - Transverse stress, location and temperature diagrams on weld centerline, 14.8 mm/s, free specimen

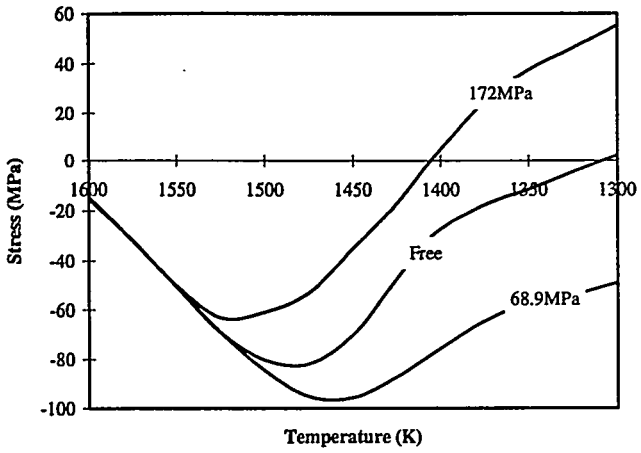

Figure 4 - Transverse stress evolution at x=15 mm, 4.23 mm/s.

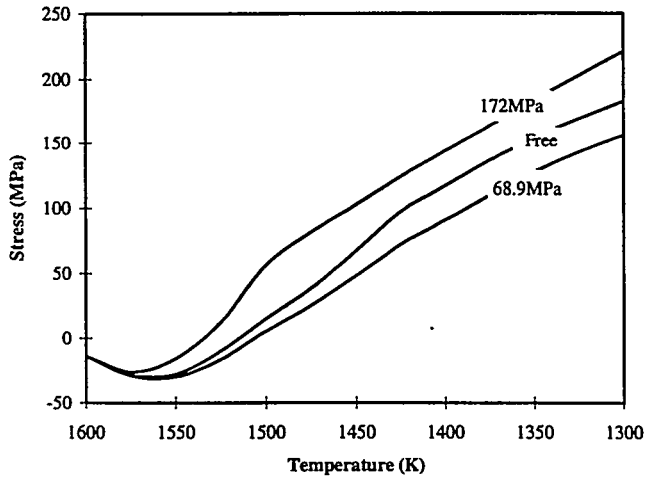

Figure 5 - Transverse stress evolution responsible for centerline cracking initiation at the starting edge of the specimen; x=-22.5mm, 14.8 mm/s.

centerline cracking normally does not initiate until the solidification front passes the middle point of the specimen. If the pre-stress is sufficiently high, cracking initiates at the start of the weld, followed by a complete specimen separation (100% cracking). Clearly, the initiation of centerline cracking is related to the development of tensile stress in the specimen. If a centerline crack does not initiate at the start of the weld, then it will not initiate until a tensile transverse stress appears again in the hump.

In the tests of low welding speed, centerline solidification cracking was observed only in the 172 MPa case. During welding, the centerline cracking was initiated somewhere between 25 to 30 mm from the starting edge of the weld. As discussed, the first half of the weld centerline is subjected to a very strong compressive stress field in the entire crack initiation temperature range except in the weld start region. Transition toward a tensile stress field begins after the solidification front passes approximately the middle point of the specimen. But only in the 172 MPa case does the tensile transverse stress field fully develops. For the stress-free specimens, the transverse stress becomes tensile only at one nodal point (x=15 mm) over the entire the weld centerline, and none in the 68.9 MPa specimens (Figure 4).

The tendency for centerline cracking under the high welding speed was found to be different. Experiment has revealed that the centerline solidification cracking, if it occurs, would initiate at the starting edge of the specimen (Figure 2). Centerline cracks were observed at the high and low loading conditions (172 MPa and stress-free specimens), while the medium loading condition (68.9 MPa) did not cause any centerline crack. Intuitively, it is difficult to comprehend why centerline cracking occurs in the stress-free specimen but not in a moderately pre-stressed specimen based on the threshold pre-stress concept. However, this phenomenon can be readily interpreted in terms of the local stress evolution at the crack initiation site located in the starting edge of the weld. Figure 5 plots the transverse stress evolution at the crack initiation site only. Compressive transverse stresses initially develop upon solidification from 1600K, then changing to tension before temperature drops to 1500K for all three pre-stress conditions. However, the tensile stress in the 68.9 MPa case is always lower than the other two cases over the entire crack initiation temperature range. Therefore, the initiation behaviors of the centerline cracking during the high welding speed tests are well explained.

Transverse Cracking. The diagrams for the longitudinal stresses were constructed using a set of nodal points close to the weld fusion line where transverse cracks were observed to initiate. They are shown in Figure 6. These diagrams give an overview of the variations in mechanical driving force in the solidification temperature range of the alloy studied. The effects of position, welding and loading conditions on the mechanical driving force are clearly presented. The longitudinal stress is compressive near the liquidus temperature. However, it always changes to a tensile stress before cooling down to 1300K, regardless of the pre-stress levels and the welding conditions.

The first striking feature shown in Figure 6 is that, unlike the transverse stress, the longitudinal stress evolution is essentially independent of the pre-stress (the mechanical constraint conditions) for the two welding speeds used in this study. This is reflected in the weldability test by the fact that the severity of transverse cracking was not influenced by the magnitude of the pre-stress (Figure 2).

The second feature observed in Figure 6 is that there are subtle differences in both the magnitude and the distribution of the longitudinal stress for the two welding speeds. In the case of high speed welds, as shown in Figure 6 (a) - (c), the build-up of the longitudinal stress quickly reached the maximum level and this maximum stress is maintained through the length of the weld, expect in the regions representing the starting and terminating craters. Since the material resistance in the locations covered by this maximum stress plateau would not vary, it is expected that the specimen would show a tendency to form transverse cracks close to the starting end of the weld, either prior to or as soon as the plateau is reached. The longitudinal stress evolution reaches the plateau at a location about 7.5 mm from the weld starting edge of the

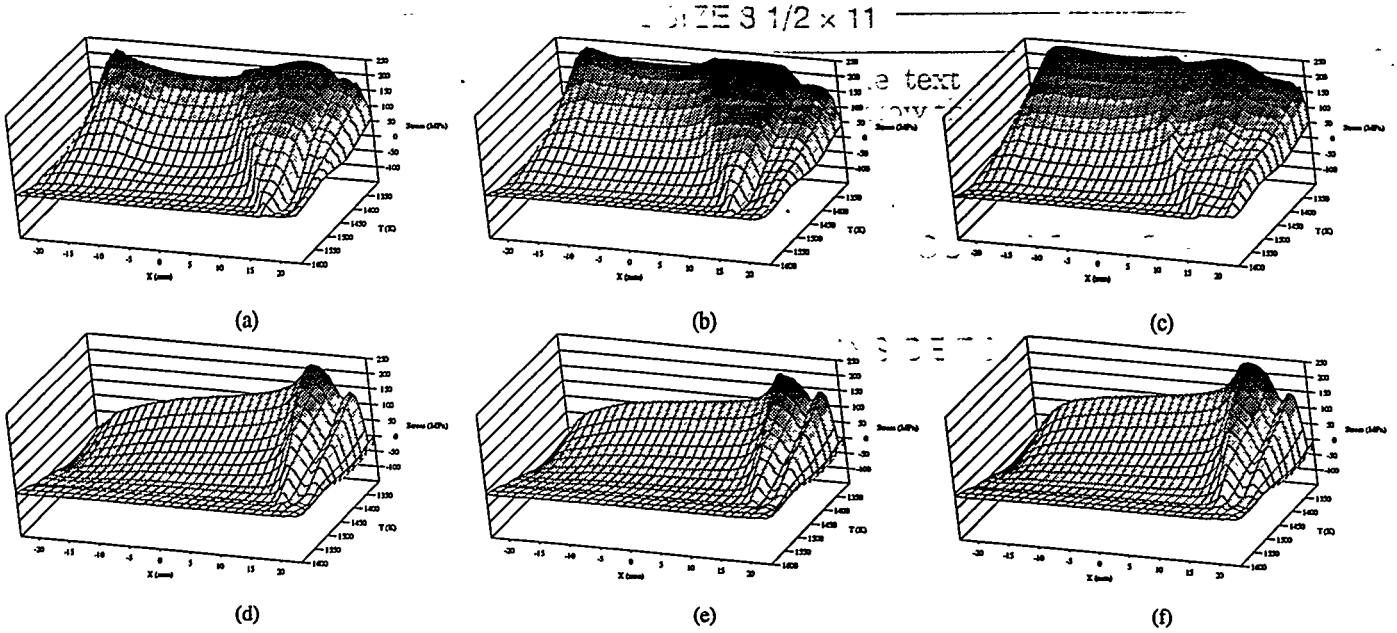

Figure 6 - Longitudinal stress, location and temperature diagrams; (a) 14.8 mm/s, free specimen (b) 14.8 mm/s, 68.9 MPa (c) 14.8 mm/s, 172 MPa (d) 4.23 mm/s, free specimen (e) 4.23 mm/s, 68.9 MPa (f) 4.23 mm/s, 172 MPa

specimen which is comparable to the location when the first transverse crack was observed (Figure 2).

In the case of low welding speed tests (Figure 6 (d) - (f)), the build of the maximum longitudinal stress occurs well into the length of the weld and close to the finishing end of the weld. This type of stress build-up made it possible for the transverse solidification cracking to initiate at locations away from the weld starting edge, as observed in the tests.

Conclusions

In this study, a finite element model that included the solidification effect in the weld pool has been used to calculate the local stresses in the solidification temperature range during the Sigmajig weldability test. The experimentally observed solidification crack initiation behaviors of a nickel based superalloy single-crystal were found to be well related to the development of local stresses at the solidification crack initiation site. The high tensile longitudinal stress at the trailing edge of the moving weld pool, which does not depend upon the pre-load condition, provides the necessary mechanical condition for the formation of transverse cracks. Both the welding speed and pre-load conditions change the development of local transverse stresses, thus affecting the formation of centerline cracks. The loading fixture in the Sigmajig test restrains the development of tensile local stress field behind the weld pool. Thus, when the pre-loading is low, the local transverse stresses at centerline crack initiation sites are actually lower than those in the fixture-free tests.

Acknowledgment

The authors thank Dr. G.M. Goodwin for many helpful discussions related to this work and Dr. B. Radhakrishnan for reviewing this paper. This research was supported by the Division of Materials Sciences, U.S. Department of Energy, under contract DE-AC05-84OR21400 with Lockheed Martin Energy Systems, and by an appointment to the Oak Ridge National Laboratory Postdoctoral Research Associates Program administered jointly by the Oak Ridge Institute for Science and Education and Oak Ridge National Laboratory.

References

1 Goodwin, G.M., *Welding J.*, 66, 33s-38s (1987).
2 Maziasz, P.J., G.M. Goodwin, C.T Liu and S.A. David, *Script Metal.* 27, 1835-1840 (1992).
3 Hibbitt, H.D. and P.V. Marcal, *Computers & Structures*, 3, 1145-1174 (1973).
4 Feng, Z., Y.Y. Zhu, T. Zacharia, R.J. Fields, P.C. Brand, H.J. Prask and J. M. Blackburn, *the 4th Int. Conf. on Trends in Welding Research.* Gatlinburg, TN (1995).
5 Feng, Z., *Welding in the World*, in press.
6 ASM International, *Metals Handbook* 10th Edition, v1 950-1006. Materials Park, OH 44073 (1990).
7 Touloukian, Y.S., R.W. Powell, C.Y. Ho and P.G. Klemens, *Thermophysical Properties of Matter*, Vol. 1 IFI/Plenum, New York (1970).
8 Touloukian, Y.S. and C.Y Ho,. (eds.) *Properties of Selected Ferrous Alloying Elements*. McGraw-Hill Book Company (1981).
9 Matsuda, F., H. Nakagawa, and K. Sorada, *Trans of JWRI* 11, 67-77 (1982).
10 Brooks, J.A., J.J. Dike and J.S. Krafcik, *Inter. Conf. Proc. on Modeling and Control of Joining Processes*, 174-185 (1993).
11 Hellwege, K-H. (ed.) *Landolt-Böenstein New Series* Group 3 v18. Springer-Verlag, Berlin (1984).
12 Ledbetter, H.M. and R.P. Reed, *J. Phys. Chem. Ref. Data* 2(3): 531-617. 1973.
13 Zacharia, T., *Welding J.*, 73, 164s-172s (1994).
14 ASM International, *Metals Handbook* 10th Edition, v1, p871, Materials Park, OH 44073 (1990).
15 Santella, M.L. and Z. Feng, This conference.